Transient Damping Method for Improving the Synchronization Stability of Virtual Synchronous Generators

Xiong, Xiaoling; Wu, Chao; Hu, Bin; Pan, Donghua; Blaabjerg, Frede

Published in:
IEEE Transactions on Power Electronics

DOI (link to publication from Publisher):
10.1109/TPEL.2020.3046462

Publication date:
2021

Document Version
Accepted author manuscript, peer reviewed version

Transient Damping Method for Improving the Synchronization Stability of Virtual Synchronous Generators

Xiaoling Xiong, *Member, IEEE*, Chao Wu, *Member, IEEE*, Bin Hu, Donghua Pan, *Member, IEEE* and Frede Blaabjerg, *Fellow, IEEE*,

***Abstract*- The virtual synchronous generator (VSG) was proposed to emulate a synchronous machine's dynamics when integrating power electronic converter-based distributed energy resources to the power grid. However, the VSG's synchronization stability during grid faults is not fully explored. The underlying mechanism of loss of synchronization (LOS) still needs to be further revealed due to VSG's nonlinear characteristics. In this paper, a step-by-step analytical method based on combining the linear and nonlinear models is proposed to analyze VSG's dynamic behaviors during a large disturbance. The relationship between the linear and nonlinear models is first brought to light, showing that the linear model is suitable for qualitative analysis to give an intuitive physical insight. Simultaneously, the latter is adopted for quantitative analysis to assess stability after a grid fault. Moreover, to avoid the conflict of the synchronization stability and the inertia response, a transient damping method is added in the active power control loop, which can simultaneously improve the synchronization stability and frequency stability. Design guidelines are also proposed to identify the parameter of the transient damping with different inertia requirements. Finally, the experimental results verify the analytical method and the theoretical analysis.**

***Index Terms*—Virtual synchronous generators, synchronization stability, transient damping, virtual inertia.**

I. Introduction

Voltage source converters (VSCs) are widely applied in renewable energy generation to connect with the conventional power grid. With the increasing penetration of renewable energy injected into the grid, the ratio of synchronous-generators (SGs)-based traditional generation decreases, which indicates that the inertia of the power grid is reduced. Thus, as the share of the VSC-based resources increases in power grids, the voltage at the point of common coupling (PCC) is vulnerable to disturbances. This paradigm shift calls for grid forming control of the VSC, which means that the VSC should have the ability to support the frequency and voltage of the power grid [1].

The implementation of grid forming control is to make VSCs perform similarly like SGs. Various control strategies have been proposed, among which the simplest and commonly used one is the *P-f* and *Q-V* droop control [2], [3]. The droop control mimics the behavior of SGs on frequency and voltage regulations, which changes the output power according to the deviation of frequency and voltage. An alternative one is the power synchronization control (PSC), which was proposed and analyzed in [4], [5] to avoid the instability caused by the phase-locked loop in the grid-following control under a weak grid [6], [7]. In fact, these two control schemes are equivalent when connecting to the grid [8]. However, these two methods lack synthetic inertia, which leads to a large frequency nadir and a high rate of change of frequency (RoCoF) during a large disturbance [9]. The large nadir and high RoCoF might be a great threat to the power system's frequency stability. Thus, the virtual inertia should be added in the PSC or droop control to decrease the frequency deviation, which can be complied with by virtual synchronous generators (VSG) control method [8], [10], [11]. Thus, this paper is going to investigate the VSCs with the VSG control strategy.

Even though the VSG control method has the frequency and voltage supporting ability, it still suffers from stability problems during different disturbances. According to the disturbance size, the stability problems can be divided into two types: small-signal stability and large-signal synchronization stability (transient stability). Substantial research efforts have been devoted to the small-signal stability analysis [12]-[14], which are basically evaluated by linearizing the system around an equilibrium operating point. The linearized model can provide clear physical insight and a better understanding of the mechanism of losing stability. However, it is not applicable if the operating point is changed by a large disturbance [15]-[17]. Although the linearizing procedure can be realized again with

Manuscript received July 21, 2020; revised October 17, 2020; accepted December 18, 2020. This work is supported by the National Natural Science Foundation of China under Grant 51707065 and part by THE VELUX FOUNDATIONS under the VILLUM Investigator Grant REPEPS (Award Ref. No.: 00016591) (*Corresponding author: Chao Wu*).

Xiaoling Xiong is with the State Key Laboratory of Alternate Electrical Power System with Renewable Energy Sources, North China Electric Power University, Beijing, 102206, China (e-mail: xiongxl1102@ncepu.edu.cn).

Chao Wu, Donghua Pan and Frede Blaabjerg are with the Department of Energy Technology, Aalborg University, Aalborg 9220, Denmark (e-mail: cwu@et.aau.dk, pan.dh@outlook.com and fbl@et.aau.dk).

Bin Hu is with the College of Electrical Engineering, Zhejiang University, Hangzhou 310027, China (e-mail: 11810031@zju.edu.cn).

This article has been accepted for publication in a future issue of this journal, but has not been fully edited. Content may change prior to final publication. Citation information: DOI 10.1109/TPEL.2020.3046462, IEEE Transactions on Power Electronics

the new operating equilibrium point, the transient stability cannot be guaranteed with the small-signal analysis method. Thus, synchronization stability, which describes the ability to maintain synchronization with the grid during grid fault, has recently received much research interests [15]-[18].

In [18], the VSC's transient stability with PSC control was analyzed and indicated no synchronization stability problem when the system has equilibrium points after the grid fault, which benefited from the first-order response of the active power control loop. However, due to the non-inertia contribution, the RoCoF was extremely high, almost a step-up response can be observed. In [8], four different types of grid-forming control are investigated and classified into two groups, non-inertia and with inertia responses. It was found that there is a conflict with the inertia response and transient stability. A mode-adaptive power-angle control was further proposed in [15], to enhance the transient stability, but the derivative measurement is hard to be implemented in practice. The transient stability was evaluated using Lyapunov's direct method in [16], [17], which swept the controller parameters one by one and derived the system's stable region. However, the frequency stability is still not mentioned. Moreover, how to use the linearized system to provide clear insight and to which extent the small-signal model can be adopted, both are not interpreted.

In the current work, the relationship between the linearized and nonlinear models should be investigated further. The detailed analyzing methods for assessing VSG's synchronization stability during grid fault are still needed to be explored. Since most existing works only aim to model the transient behaviors, an effective control method to improve the synchronization stability should be further studied. Besides, the dynamics of frequency response during the grid faults are overlooked, which is a significant indicator of the grid-forming control. In order to solve these potential problems, the specific contributions of this paper can be concluded as follows:

1. Based on combining the linearized model and the nonlinear model of the system, a step-by-step analytical method is proposed for analyzing the synchronization stability. The relationship between the linear and nonlinear model is first revealed. The former one is used for qualitative analysis to give clear physical insight and better understanding. Additionally, the latter is adopted for quantitative analysis to assess stability by using the trajectories in the phase plane.
2. A transient damping method is introduced to enhance synchronization stability and frequency stability. The RoCoF and maximum frequency variation during the transient period are first considered.
3. Based on the combined analytical method, the synchronization stability of the VSG with adding the transient damping method is studied in details, and guidelines for parameter design are given.

This paper is organized as follows. The system description and the equivalent analytical model of the VSG are presented in section II. The combined analytical method for studying synchronization stability is elaborated in section III in details, where the relationship of the linearized and nonlinear model is revealed. Section IV introduces a transient damping method to improve synchronization stability and decrease the maximum frequency variation during the grid fault. The detailed parameter design process of the transient damping is also derived. Section V shows the experimental results, and the conclusions are drawn in section VI.

II. SYSTEM DESCRIPTION

Fig.1 shows the general system diagram of a three-phase grid-connected VSG. The traditional grid model with a Thevenin equivalent circuit, i.e., an inductance L_g behind an infinite bus, is adopted [4], [5]. Here, $\mathbf{V}_g$ and $\mathbf{V}_{pcc}$ represent the voltage space vectors for the grid and the point of common coupling (PCC), respectively, giving $\mathbf{V}_g = V_g e^{j\omega_g t}$ (usually the angular frequency $\omega_g = \omega_0$) and $\mathbf{V}_{pcc} = V_{pcc} e^{j\theta_{pcc}}$. L_f and C_f represent the VSG's output filter, P and Q are the output active power and the reactive power of the VSG, respectively. $\mathbf{I}_g$ is the vector of the current injected into the grid. The dc-link voltage is usually controlled by a front-end converter for a high voltage dc system [4], [19], or controlled by an energy storage converter for integrating the renewable energy to the grid [10], [11], [20], [21]. Hence, the dc voltage can be assumed to be constant when analyzing the synchronization stability of VSG [8], [15]-[18].

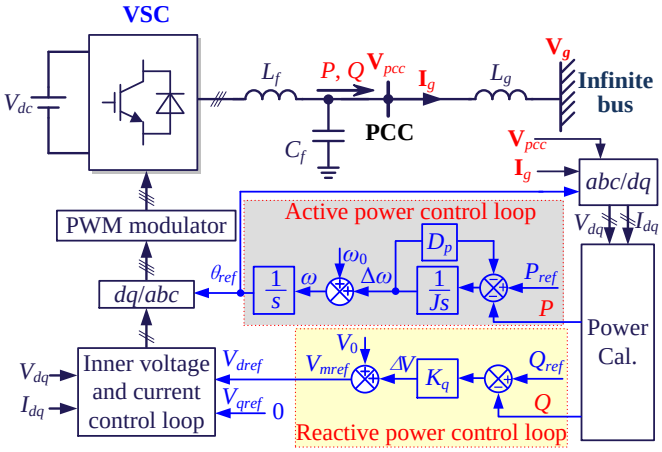

Fig. 1. General system diagram of a three-phase grid-connected VSG.

As shown in Fig. 1, P_{ref} and Q_{ref} are active and reactive power references, respectively. the objective of VSG control is to generate the phase and the voltage amplitude reference for the PCC voltage, i.e., $\mathbf{V}_{ref} = V_{mref} e^{j\theta_{ref}}$. An inner voltage and current control loop is employed to regulate $\mathbf{V}_{pcc}$ to track $\mathbf{V}_{ref}$, and implementing an over-current protection. Usually, the inner loop's bandwidth is much higher than that of the outer power control loop [22], [23]. Due to the decoupled timescales, the inner control loop gain can be regarded as unity gain with an ideal PCC voltage reference tracking, as the synchronization issues are mainly determined by the outer power control loop [8], [15-18]. Hence, $V_{pcc} = V_{mref}$, $\theta_{pcc} = \theta_{ref}$, the VSG is operated as a voltage-controlled voltage source. This simplification has

This article has been accepted for publication in a future issue of this journal, but has not been fully edited. Content may change prior to final publication. Citation information: DOI 10.1109/TPEL.2020.3046462, IEEE Transactions on Power Electronics

been validated in previous research works [8], [15-18], [24], [25], thus, it will be further used without extra verification in this paper. If the grid fault triggers the current protection, the control will be changed to grid-following control method, and the transient stability has been studied in [26], [27]. Therefore, this paper only focuses on the transient problems that won't trigger the overcurrent protection.

According to Fig. 1, ω is defined as the angular frequency of the VSG, and $\omega = \omega_0 + \Delta\omega$ can be easily obtained. From this, the active power control law can be written as

$$\omega = \omega_0 + \frac{1}{Js + D_p} \cdot \left(P_{ref} - P\right) \tag{1}$$

where J and D_p are the virtual inertia and the gain of frequency governor, respectively.

The reactive power-voltage (Q-V) droop control is employed [15], [28] for the reactive power control loop, and the transfer function of which is given by

$$V_{mref} = V_0 + K_q \left(Q_{ref} - Q\right) \tag{2}$$

where K_q is the controller gain of reactive power.

Defining δ as the power angle, which is the phase difference between $\mathbf{V}_{pcc}$ and $\mathbf{V}_g$, i.e., $\delta = \theta_{pcc} - \theta_g = \theta_{ref} - \omega_g t$. Thus, P and Q can be derived as

$$P = \frac{3}{2} \cdot \frac{V_{pcc} V_g \sin\delta}{X_g} \tag{3}$$

$$Q = \frac{3}{2} \cdot \frac{V_{pcc}^2 - V_{pcc} V_g \cos\delta}{X_g} \tag{4}$$

where $X_g = \omega_0 L_g$.

Substituting (4) into (2) and considering $V_{pcc} = V_{mref}$, the relationship between V_{pcc} and δ can be derived, which is given in (5) at the bottom of this page.

According to the above analysis, the VSG's equivalent analytical model can be obtained, as shown in Fig. 2. Based on this model, the dynamics of VSG during the transient period will be analyzed in the following sections.

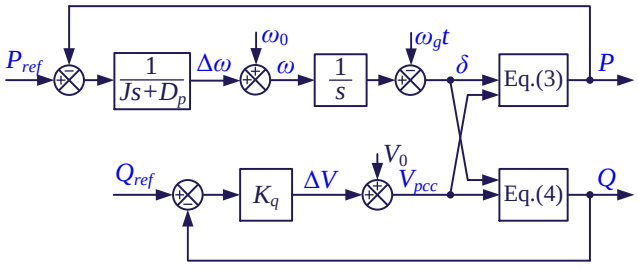

Fig. 2. The equivalent analytical model of the grid-connected VSC.

III. Synchronization Stability Analysis Method

A. *Types of Transient Issues*

Substituting (5) into (3), the $P-\delta$ curves are obtained, as plotted in Fig. 3. As shown by the solid line, the VSG operates initially at point a, where $P = P_{ref}$ in the steady-state. After the disturbance occurs, there are basically two types of transient problems, i.e., the equilibrium point exists or not [8], [18], which depends on the depth of the grid voltage sag, as it is shown in Fig. 3. The dashed green line shows there is no equilibrium point after the grid voltage sag. The synchronization cannot be guaranteed just only by improving the control strategies or controller design. Thus, this type will not be included in this paper.

In Fig. 3, the dashed red line illustrates the existence of the equilibrium point after a disturbance, which is of concern in this work. For example, the VSG will switch from point a to point d when the grid voltage sag is 20%. The point b and b_1 represent the two equilibrium points, respectively, and the corresponding power angles are denoted as δ_e and δ_{ce}. If δ exceeds δ_{ce} and then diverges to infinite, which would cause the loss of synchronization (LOS) with the grid. Thus, δ_{ce} is called the critical power angle. General speaking, to guarantee the stability of a linear system, we need to check the following two steps:

1) Check the existence of an equilibrium point after the disturbance.

2) Check the small-signal stability of the equilibrium point.

However, due to the nonlinear relationships in Fig. 2, the transient response after a large disturbance might differ from the linear system. Thus, even if 1) and 2) are satisfied, the LOS might occur during the transient period.

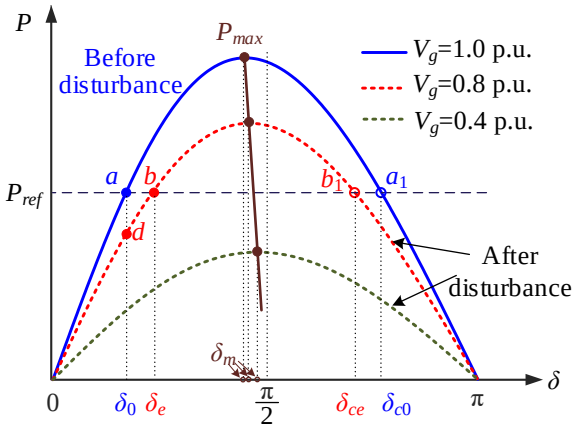

Fig. 3. P-δ curves with different grid voltage sags, solid line: before disturbance, dashed line: after a disturbance when the grid voltage drops 20% in red and drops 60% in green.

$$V_{pcc}(\delta) = \frac{1.5K_qV_g\cos\delta - X_g + \sqrt{\left(X_g - 1.5K_qV_g\cos\delta\right)^2 + 6K_qX_g\left(V_0 + K_qQ_{ref}\right)}}{3K_q} \tag{5}$$

This article has been accepted for publication in a future issue of this journal, but has not been fully edited. Content may change prior to final publication. Citation information: DOI 10.1109/TPEL.2020.3046462, IEEE Transactions on Power Electronics

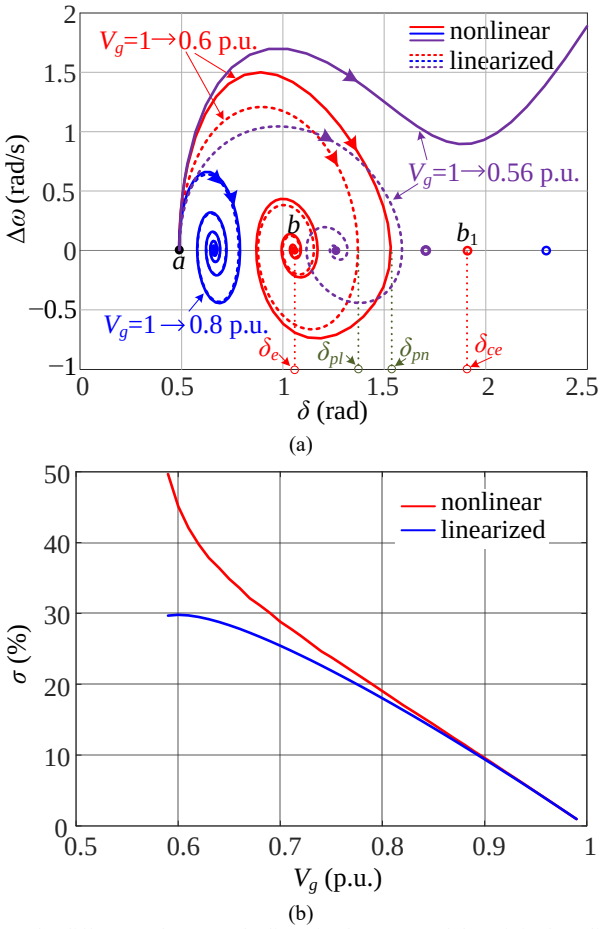

Fig. 4. The differences between the linearized system and the original nonlinear system with different grid voltage sag and J = 20 p.u., D_p = 20 p.u., (a) the trajectories in the phase plane and (b) The overshoot of power angle with different grid voltage sag.

B.Combining the Linearized and nonlinear models

Although the nonlinear system is stable in the neighborhood of b, how large of this neighborhood is so far not known. As shown in Fig. 4(a), the trajectories of the nonlinear system in Fig.2 and the corresponding linearized system are both plotted using the parameters in Table I in Section V. From there, it can be seen that the transient response of the nonlinear system is approximately the same as that of the linearized system when the grid voltage drops 20%. Yet, there is a large error for the grid voltage dropping 40% and 44%. The linearized model even gives a wrong stability assessment when the grid voltage dropsto 0.56 p.u.. It indicates that a linearized system cannot be used for the stability analysis when the voltage drops a lot since the system is a strictly nonlinear system during the grid faults. A quantitative analysis between the linear and nonlinear models during different grid voltage sags is shown in Fig. 4(b). Taking V_g drops from 1 p.u. to 0.6 p.u. in Fig. 4(a) as an example, δ_{pj} (j = l for the linearized system and j = n for the nonlinear system), is the peak of δ during the transient period. The power angle overshoot is denoted as σ, gives as $\sigma = (\delta_{pj} - \delta_e)/\delta_e$. It can be seen that the power angle overshoot of the nonlinear model will deviate a lot from the linearized model when the voltage sag is larger than 0.2 p.u.. That is the limitation of the linearized small-signal model when analyzing the transient process of a nonlinear system.

Fortunately, suppose the nonlinear system is stable during the transient period; in that case, it will finally arrive at the neighborhood of b, so the trajectory for the nonlinear system has a similar response trend as the linearized system, i.e., a shrinking spiral converging to b (if the system has a pair of conjugate eigenvalues). Thanks to this feature, the linearized system can be used for qualitative analysis, such as analyzing the overshoot and the damping ratio ζ. A larger ζ leads to a smaller overshoot for a linear second-order system, and it also applies to the nonlinear system. In order to prove this quantitatively, the angle overshoot with different damping ratios has been plotted in Fig. 5. The two power angle overshoots from the linear and nonlinear models are distinct because the voltage drop is large. However, the changing trend of overshoot with the damping ratio is the same for the two models. In other words, a larger ζ is designed for the linearized system to make δ_{pl} smaller, δ_{pn} will correspondingly become smaller, which can improve the transient stability of the system. To make sure the synchronization stability, δ_{pn} must not exceed δ_{ce} during the transient period, thus improving the system's damping ratio becomes significantly essential.

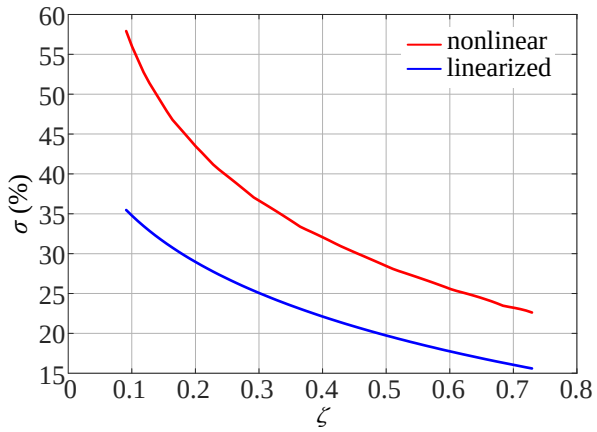

Fig. 5. The overshoot of power angle for the linearized system and the original nonlinear system with different damping ratios when V_g= 1→ 0.6 p.u..

Based on the above analysis, it can be concluded that the linearized model can be applied for the qualitative analysis to give intuitive physical insight into the synchronization stability during grid faults. The nonlinear model is inevitably used for the quantitative analysis to make an accurate assessment of the synchronization stability. Therefore, to make sure that the synchronization stability of the VSG is obtained, despite the two steps presented in part A, another step should be checked, giving as

3) During the grid fault, the power angle δ should not exceed δ_{ce} so that the power angle's transient stability can be guaranteed. The linear system can be used for the qualitative analysis, and the numerical study of the nonlinear system should be adopted to obtain the actual behaviors.

Then we need to check the three requirements. Only if all of them are satisfied, the LOS definitely will not happen. However,

This article has been accepted for publication in a future issue of this journal, but has not been fully edited. Content may change prior to final publication. Citation information: DOI 10.1109/TPEL.2020.3046462, IEEE Transactions on Power Electronics

if the conditions in 1) or 2) are not achieved, there is no need to analyze the transient stability in 3), as the system will undoubtedly lose its stability.

IV. Introducing a Transient Damping

Although high virtual inertia was unexpected from the transient stability perspective, it is always emulated in the VSG to support the system frequency. Hence, there is an urgent demand to stabilize the VSG with a high-inertia contribution.

In order not to alter the desired steady-state characteristics and not to deteriorate the frequency performance, transient damping can be added to improve the transient response. The transient damping is introduced into the active power control loop, by feeding back the frequency difference between the VSG and the grid, like shown in Fig. 6. Due to $\omega = \omega_g$ in steady-state as the system is synchronized with the grid at last, then the additional path does not influence the steady-state characteristics. Here, it should be noted that a phase-locked loop (PLL) is employed to measure the grid's frequency, the bandwidth of which is designed much higher in order to avoid affecting the transient behaviors of the power control loop.

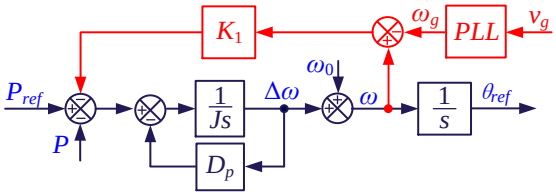

Fig. 6. The transient damping introduced into the active power control loop.

From Fig. 6, the active power control law can be derived, which is different from (1), giving as

$$\omega = \frac{\left(Js + D_p\right)\omega_0 + P_{ref} - P + K_1\omega_g}{Js + D_p + K_1} \tag{6}$$

here, $\omega = \omega_g$ is achieved at the steady-state when the system is stable, substituting it to (6), which becomes the same as (1), indicating the steady-state's frequency deviation is the same. In order to analyze the VSG's synchronization stability, the three analytical steps presented in section III are applied in the following part.

A. Existence of the Equilibrium Points

According to the previous description, it can be known that the system is a second-order nonlinear system, the dynamics of which can be represented in the standard form. Suppose $\boldsymbol{x}$ is the state variable vector defined as $\boldsymbol{x} = [x_1, x_2]^T$. Here, superscript T represents the transposition of a matrix or vector and $x_1 = \delta$, $x_2 = \Delta\omega$. Thus, we can obtain

$$\begin{bmatrix} \dot{x}_1 \\ \dot{x}_2 \end{bmatrix} = \begin{bmatrix} x_2 + \omega_0 - \omega_g \\ -\dfrac{D_p + K_1}{J}x_2 - \dfrac{3V_g F(x_1)}{2JX_g} + \dfrac{P_{ref}}{J} - \dfrac{K_1\left(\omega_0 - \omega_g\right)}{J} \end{bmatrix} \tag{7}$$

where dot $(\cdot)$ denotes the time derivative, and $F(\delta) = V_{pcc}(\delta)\sin\delta$.

By setting all the differential items in (7) to zero, the equilibrium point $\boldsymbol{x_e} = [\delta_e, \Delta\omega_e]^T$ can be obtained. This obviously implies $\Delta\omega_e = \omega_g - \omega_0$ and δ_e must satisfy that

$$\frac{3}{2}\cdot\frac{V_g V_{pcc}\left(\delta_e\right)\sin\delta_e}{X_g} = P_{ref} - D_p\left(\omega_g - \omega_0\right) \tag{8}$$

It can be found the equilibrium points are not dependent on K_1, indicating again the transient damping method does not affect the steady-state. Therefore, if and only if the maximum output active power of VSG, i.e., P_{max}, is larger or equal to P_{ref} (assuming $\omega_g = \omega_0$ at stead-state for simplifying describing), the equilibrium point exists. For the system in Table I in Section V, the critical grid voltage is 0.55 p.u., then V_g dropping to 0.6 p.u. is tested in this paper to ensure the existence of the equilibrium points.

B. Small Signal Stability of the Equilibrium Points

In order to ensure the nonlinear system can converge to the just derived $\boldsymbol{x_e}$ after a transient period and can finally operate at $\boldsymbol{x_e}$ stably, we must first assure that $\boldsymbol{x_e}$ is small-signal stable. This can be done by investigating the dynamical behaviors of the linearized system around $\boldsymbol{x_e}$, i.e., to exam the eigenvalues of the Jacobian $\boldsymbol{J}(\boldsymbol{x_e})$, which is derived as

$$\boldsymbol{J}(\boldsymbol{x_e}) = \begin{bmatrix} 0 & 1 \\ J_{21} & -\left(D_p + K_1\right)/J \end{bmatrix} \tag{9}$$

where J_{21} is calculated as

$$J_{21} = \left.\frac{\partial f_2}{\partial x_1}\right|_{x = x_e} = -\frac{3V_g}{2JX_g}F'\left(\delta_e\right) \tag{10}$$

and $F'(\delta)$ can be derived as

$$\begin{aligned} F'\left(\delta\right) = \frac{dF}{d\delta} &= V_{pcc}\left(\delta\right)\cos\delta \\ &- \frac{3K_q V_g V_{pcc}\left(\delta\right)\sin\delta}{2X_g + 3K_q\left(2V_{pcc}\left(\delta\right) - V_g\cos\delta\right)}\sin\delta \end{aligned} \tag{11}$$

Then, the eigenvalues of the Jacobian are found by specifically solving the characteristic equation, $\det[\lambda\boldsymbol{I} - \boldsymbol{J}(\boldsymbol{x_e})] = 0$, where $\boldsymbol{I}$ is the unit matrix. The solutions are calculated as

$$\lambda_{1,2} = \frac{-\left(D_p + K_1\right) \pm \sqrt{\left(D_p + K_1\right)^2 + 4J_{21}J^2}}{2J} \tag{12}$$

Only if all the eigenvalues have a strictly negative real part, $\boldsymbol{x_e}$ is stable, and the original nonlinear system is thus small-signal stable in the neighborhood of $\boldsymbol{x_e}$.

Suppose when $\delta = \delta_m$, $P(\delta_m) = P_{max}$, as shown in Fig. 3, and thus $\frac{dP}{d\delta}|_{\delta_m} = 0$. According to (3), we can get $F'\left(\delta_m\right) = 0$. Substituting it to (10), $J_{21}(\delta_m) = 0$ is derived. From Fig. 3, it can be found that P is monotonically increasing with δ when

This article has been accepted for publication in a future issue of this journal, but has not been fully edited. Content may change prior to final publication. Citation information: DOI 10.1109/TPEL.2020.3046462, IEEE Transactions on Power Electronics

$\delta < \delta_m$ and monotonically decreasing with δ when $\delta > \delta_m$. Therefore, when $\delta < \delta_m$, $\frac{dP}{d\delta} > 0$, then $F'(\delta) > 0$, as a result, $J_{21}(\delta) < 0$ is obtained. Similarly, when $\delta > \delta_m$, $J_{21}(\delta) > 0$ can be derived. These relationships between J_{21} and δ are also illustrated in Fig. 7.

If $P(\delta_m) = P_{ref}$, there is only one equilibrium point, such as $\delta_e = \delta_{ce} = \delta_m$. As $J_{21}(\delta_m) = 0$, $\lambda_1 = -(D_p+K_1)/J$, $\lambda_2 = 0$ can thus be derived. $\boldsymbol{x_e}$ is critically stable and can easily lose its stability with a small perturbation, which is regarded as unstable. If $P(\delta_m) > P_{ref}$, two equilibriums exist, such as the points b and b_1 in Fig. 7, meanwhile $\delta_e < \delta_m$, $\delta_{ce} > \delta_m$. According to the above analysis and Fig. 7, $J_{21}(\delta_e) < 0$ and $J_{21}(\delta_{ce}) > 0$ can be obtained. According to (12), it can be derived that both λ_1 and λ_2 have a negative real part for b, but one of the eigenvalues has a positive real part for b_1. Thus, point b is small-signal stable but point b_1 is not. Therefore, from the small-signal stability viewpoint, there must be one equilibrium point b certainly stable as long as $P_{max} > P_{ref}$.

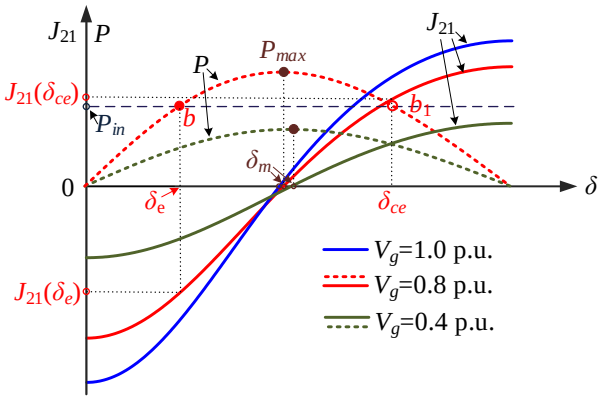

Fig. 7. J_{21}-δ and P-δ curves with different grid voltage sags. Solid line: J_{21}-δ curves, dashed line: P-δ curves with the nominal grid voltage in blue, the grid voltage drops 20% in red and drops 60% in green.

C. *Qualitative Analysis of Synchronization Stability*

Firstly, the linearized system is employed for the qualitative analysis of synchronization stability. To identify the damping ratio, the relationship between P and δ shown in Fig. 2 should be linearized firstly around b, given as

$$\hat{P} = \frac{3V_g}{2X_g} F'(\delta_e)\cdot\hat{\delta} \quad \overset{define}{\Rightarrow} \quad G_p = \frac{3V_g}{2X_g} F'(\delta_e) \tag{13}$$

where cap (^) represents the small variations, G_p is the approximate gain between P and δ evaluated at b. From (11) and (13), it can be derived that G_p is related to the system parameters, such as V_g, X_g, P_{ref}, and K_q. For a given condition, these parameters are constant. Thus G_p is constant and $G_p > 0$ (as $F'(\delta_e) > 0$). Then substituting (13) to Fig. 2, for a small perturbation of P_{ref}, the dynamic of δ and ω, can be described in the s-domain as

$$\frac{\hat{\delta}}{\hat{P}_{ref}} = \frac{1}{Js^2 + (D_p + K_1)s + G_P} \tag{14}$$

$$\frac{\hat{\omega}}{\hat{P}_{ref}} = \frac{s}{Js^2 + (D_p + K_1)s + G_P} \tag{15}$$

The damping ratio of the system is derived as

$$\zeta = \frac{D_p + K_1}{2\sqrt{JG_P}} \tag{16}$$

Since G_p is constant with the given system condition, ζ is determined by D_p, K_1 and J. Therefore, a larger D_p, K_1 and a smaller J are expected to reduce the power angle overshoot and thus to improve the synchronization stability. Generally, D_p is the frequency governor's gain in VSG, which is always designed fixed according to the grid codes; otherwise, it will change the desired droop characteristics. Meanwhile, a smaller J can enhance transient stability, but it deteriorates the frequency response.

Assuming that there is a step change of the power reference (the grid voltage change can be equivalent to the power reference change), the Laplace form is 1/s. Thus, according to (15) the response of the frequency in the s-domain can be deduced as,

$$\hat{\omega} = \frac{s}{Js^2 + (D_p + K_1)s + G_P}\frac{1}{s} = \frac{1}{Js^2 + (D_p + K_1)s + G_P} \tag{17}$$

Using damping and the undamped natural frequency, rewrite (17) in the standard form as,

$$\hat{\omega} = \frac{\omega_n^2 / G_p}{s^2 + 2\zeta\omega_n s + \omega_n^2} \tag{18}$$

where $\omega_n^2 = G_p / J$, $2\zeta\omega_n = (D_p + K_1)/J$.

Thus, the frequency response in the time domain can be derived as,

$$\hat{\omega} = \frac{1}{G_p}\frac{\omega_n^2}{\sqrt{1-\zeta^2}} e^{-\zeta\omega_n t} \sin\left(\sqrt{1-\zeta^2}\,\omega_n t\right) \tag{19}$$

Thus, the RoCoF is deduced as,

$$\text{RoCoF} = \frac{d\hat{\omega}}{dt} = \frac{1}{G_p}\frac{\omega_n^2}{\sqrt{1-\zeta^2}} e^{-\zeta\omega_n t} \sin\left(\beta - \sqrt{1-\zeta^2}\,\omega_n t\right) \tag{20}$$

where $\sin\beta = \sqrt{1-\zeta^2}$.

When t=0, the maximum RoCoF is achieved during the transient process and it can be calculated as,

$$\text{RoCoF}|_{\max} = \frac{1}{G_p}\frac{\omega_n^2}{\sqrt{1-\zeta^2}} \sin(\beta) = \frac{1}{J} \tag{21}$$

From this, it can be seen that the maximum RoCoF is only relevant to the inertia J but has no relationship with the damping coefficient D_p and K_1.

When the derivative of frequency is equal to zero, the maximum frequency variation can be obtained, given as,

This article has been accepted for publication in a future issue of this journal, but has not been fully edited. Content may change prior to final publication. Citation information: DOI 10.1109/TPEL.2020.3046462, IEEE Transactions on Power Electronics

$$\hat{\omega}|_{\max} = \omega_n e^{-\frac{\zeta}{\sqrt{1-\zeta^2}}\arcsin\left(\sqrt{1-\zeta^2}\right)} \approx \sqrt{\frac{G_p}{J}} e^{-\zeta} \tag{22}$$

The maximum frequency has an inverse ratio with the inertia and damping, which means that the maximum frequency variation will decrease with the increase of inertia and damping. However, increasing the virtual inertia is unexpected from the perspective of the transient stability. Therefore, increasing the transient damping is flexible, entirely avoiding the conflict between frequency stability and synchronization stability.

D. Quantitative Analysis of Synchronization Stability

The numerical study based on (7), i.e., the trajectories in the phase plane, is used to obtain the nonlinear system's actual behaviors. From the previous analysis, the additional path increases the damping ratio, and a larger K_1 leads to a larger damping ratio, which benefits the transient stability but also reduces the frequency variation during the grid fault. The transient behavior's influence is further illustrated in Fig. 8 based on the nonlinear system in (7). It can be observed that without the additional path, a LOS occurs when the grid voltage drops from 1 p.u. to 0.6 p.u. with J = 20 p.u., due to the poor damping dynamics. Decreasing J to 10 p.u. can remove this instability due to an increased ζ reduces the power angle overshoot. However, the frequency response becomes worse due to the smaller inertia. Since the frequency of VSG is the sum of ω_0 and $\Delta\omega$, then the important frequency performance indices are determined by $\Delta\omega$. For example, the peak angular frequency during the transient period is proportional to the maximum deviation of $\Delta\omega$, which is denoted as $\Delta\omega_{max}$ (is proportional to $\hat{\omega}|_{max}$ in (22)), as shown in Fig. 8. The RoCoF is equal to the change rate of $\Delta\omega$. Fig. 8 also shows that a smaller J deteriorates the frequency stability due to the larger $\Delta\omega_{max}$ and RoCoF.

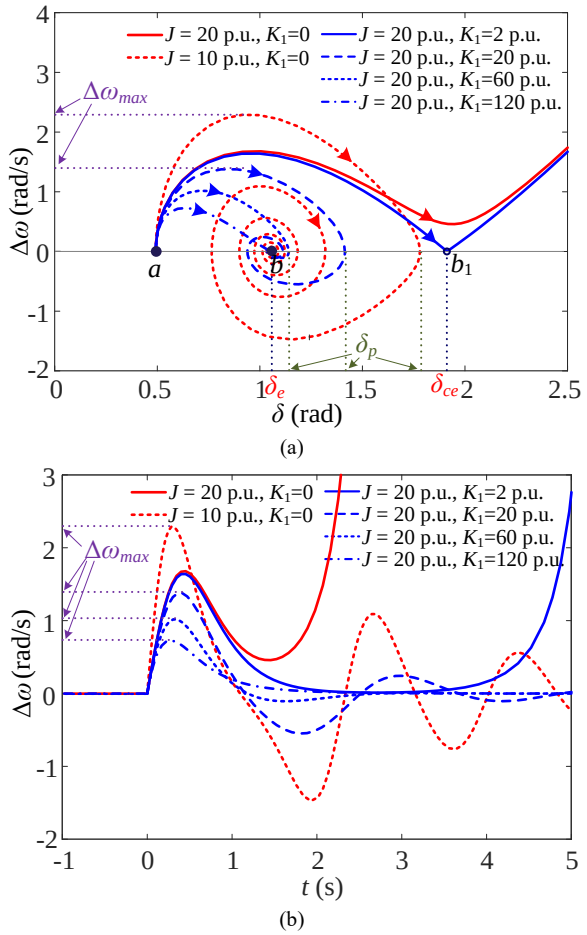

Fig. 8. The influence of parameters K_1 and J on transient performances of the VSG when V_g = 1→ 0.6 p.u., (a) the trajectories of the nonlinear system in the phase plane and (b) the responses of $\Delta\omega$.

Under the same condition, the power angle overshoot and $\Delta\omega_{max}$ are reduced with an increase of K_1, due to the increased ζ. Even an overdamped response of δ can be achieved using a sufficiently large K_1, i.e., K_1 = 120 p.u.. Moreover, the maximum deviation $\Delta\omega_{max}$ decreases with increasing of K_1, which enhances the frequency stability. Therefore, a larger K_1 is expected to reduce the power angle overshoot and improve synchronization stability. Otherwise, instability can occur if K_1 is not large enough, i.e., K_1 = 2 p.u.. The system suffers from a poorly damped dynamics, which causes δ to exceed δ_{ce}.

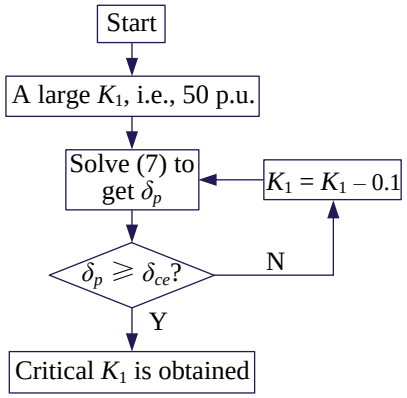

Fig. 9. Iterative calculation procedure for detecting the critical value of K_1.

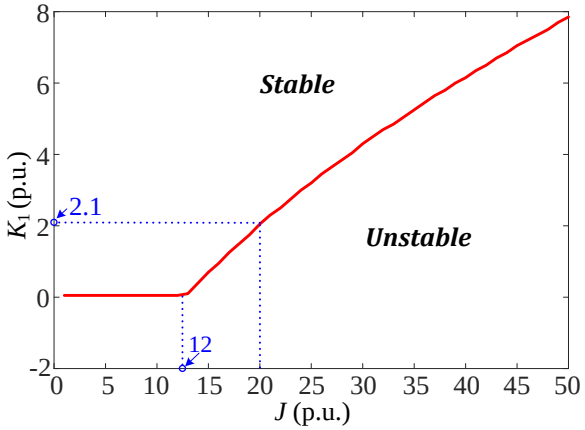

Fig. 10. The stability boundary regarding K_1 versus J when V_g = 1→ 0.6 p.u.

The transient stability benefits a lot with a large K_1, but extremely large K_1 is also undesirable for most practical purposes, as it slows down the dynamics of the active power loop. The stability boundary with parameter K_1 needs to be

This article has been accepted for publication in a future issue of this journal, but has not been fully edited. Content may change prior to final publication. Citation information: DOI 10.1109/TPEL.2020.3046462, IEEE Transactions on Power Electronics

found, which is also beneficial design information for engineers to identify how far or close the system is from the LOS region. As only if δ exceeds δ_{ce}, LOS can occur. Thus, as long as the maximum power angle overshoot δ_p does not exceed δ_{ce}, the synchronization stability can be guaranteed.

D_p and K_q are usually designed fixed according to the grid codes [12]. Then, for each specified virtual inertial J, the critical value of K_1 for a stable operation can be found with the calculation procedure shown in Fig. 9. K_1 is initialized with a large value, i.e., K_1 = 50 p.u. to make sure the system operates stably under the specified condition, and then K_1 is decreased with a small step and find the maximum power angle δ_p during every iterative calculation, until δ_p exceeds δ_{ce}. The calculation step is set at 0.1, determined by a trade-off between the accuracy of the critical value and the computional burden. The procedure is then repeated to find all the critical values of K_1 under different J. The results are shown in Fig.10, where the stable and unstable regions of operation are located above and below the boundary line. It can be seen that with the increase of J, the minimum allowed K_1 for the stable operation increases. For example, if $J < 12$ p.u, the additional path is unnecessary, but with $J \geq 12$, the additional damping must be introduced. Such as, if J = 20 p.u, then $K_1 > 2.1$ p.u. must be adopted. Hence, adding a larger K_1, higher inertia becomes viable. Adjusting K_1 and the inertia together can simultaneously guarantee synchronization stability and frequency stability.

It is worth noting that many damping techniques for VSG control have been proposed in other literature, which can be generally divided into two categories. Category 1: the damping coefficient is mixed with the droop coefficient [10], [11] [14], [29], just like D_p in Fig. 1 in this paper, which is a simple and basic solution in the VSG control. However, the combined droop function with the damping strategy could be problematic in scenarios where the damping is not sufficiently large, the system suffers from poorly damped dynamics. If increasing D_p to increase the damping ratio, which will alter the droop function and change the steady-state characteristics. This is also the reason for introducing the transient damping method in this paper, which increases the damping ratio during the transient period, but not to change the steady-state performance.

Category 2: To avoid changing the steady-state characteristics, more sophisticated damping solutions have been reported in the literature, which was thoroughly reviewed in [30]. An evolving damping solution was proposed in [31], [32], by feeding back the angular frequency of the VSG with a high-pass filter, which is an attractive solution as it also just provides damping during the transient period. However, a modification on the damping mechanism will alter the swing equation, leading to a higher-order dynamic response [5] and thus change the transient behavior. The motivation of this manuscript is to reveal the relationship between the linearized system and the nonlinear system, establishing a combined qualitative and quantitative analysis method for the synchronization stability of the VSG, by focusing on the basic control scheme. For more sophisticated damping techniques, further studies can be easily drawn based on the established methodology in this paper.

E. *Other Types of Grid Faults*

The grid faults generally include symmetrical grid faults and asymmetrical grid faults. In this paper, the symmetrical three-phase grid voltage dips are mainly analyzed since they are more severe than other asymmetrical grid faults. The same analytical methods can be applicable to other types of symmetrical grid faults, even power oscillations in [33]. For the asymmetrical grid faults, the only difference is that the symmetrical components theory should first be used to extract the positive, negative, and zero-sequence components.

Single line-to-ground (SLG) fault, double line-to-ground (DLG) fault, line-to-line (LL) fault, as shown in Fig. 11, are the main asymmetrical grid faults. Take the SLG fault as an example, the most severe case is the interfaced impedance Z_F = 0, then the three-phase grid voltage after the SLG fault in per-unit can be expressed in the phasor domain as,

$$\begin{cases} v_{Fa} = 0 \\ v_{Fb} = e^{-j2\pi/3} \\ v_{Fc} = e^{-j4\pi/3} \end{cases} \tag{23}$$

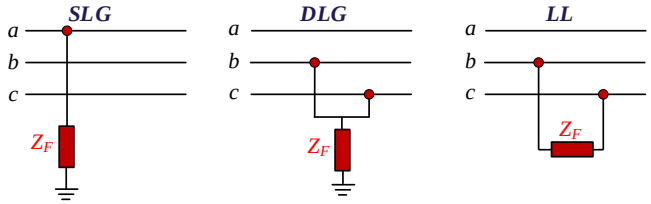

Fig. 11. Phase configurations at the fault location for a single line-to-ground (SLG), a double line-to-ground (DLG), and a line-to-line (LL) fault [34].

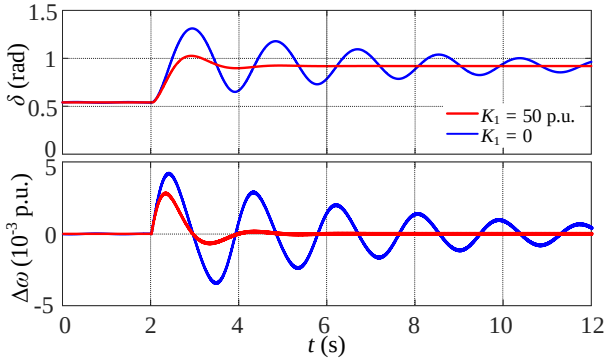

Fig. 12. The responses of δ and $\Delta\omega$ when a single line-to-ground (SLG) fault occurs (J = 20 p.u).

Firstly, using the symmetrical components theory to extract positive-sequence, negative-sequence, and zero-sequence components, which can be expressed as,

$$\begin{bmatrix} v_F^+ \\ v_F^- \\ v_F^0 \end{bmatrix} = \frac{1}{3}\begin{bmatrix} 1 & \alpha & \alpha^2 \\ 1 & \alpha^2 & \alpha \\ 1 & 1 & 1 \end{bmatrix}\begin{bmatrix} v_{Fa} \\ v_{Fb} \\ v_{Fc} \end{bmatrix} \tag{24}$$

where $\alpha = e^{j2\pi/3}$, v_F^+ and v_F^- are the phasor of positive-

This article has been accepted for publication in a future issue of this journal, but has not been fully edited. Content may change prior to final publication. Citation information: DOI 10.1109/TPEL.2020.3046462, IEEE Transactions on Power Electronics

and negative-sequence voltage, v_F^0 is the zero-sequence voltage.

Substituting (24) into (23), the magnitude of the three voltages can respectively be deduced as,

$$\left|v_F^+\right|=0.67,\quad \left|v_F^-\right|=0.33,\quad \left|v_F^0\right|=0.33 \tag{25}$$

It can be seen that $|v_F^+|$ is higher than 0.6, better synchronization stability can be obtained than the symmetrical voltage dropping to 0.6 p.u.. Since there is no corresponding control strategy to suppress the negative and zero-sequence, these components will not affect the synchronization stability. Suppose there are some specific requirements of the negative sequence current injection; in that case, the detailed analysis is similar to the positive-sequence study, which can be seen in [34] and not repeated in this paper, because the primary analytical method is the same.

In order to verify the statement, an asymmetrical SLG fault is carried out with the simulation platform in Matlab/Simulink. Only the phase *a* is decreased to 0 p.u., the responses of δ and $\Delta\omega$ are shown in Fig. 12. It can be seen that the system is stable under the worst SLG grid fault, but it has a long period of oscillation due to the large inertia. The transient damping method is also useful to suppress the asymmetrical fault oscillations, which demonstrates that the transient damping method is also effective during other types of grid faults.

V. Experimental Verification

To verify the effectiveness of the theoretical synchronization stability analysis and the improved transient damping method, experiments based on Control-hardware-in-loop (CHIL) are carried out in the lab. The hardware platform of CHIL verification is shown in Fig. 13. The main circuit of the VSG is emulated in Typhoon HIL 602+ with the time step of 1μs. Controllers of VSG are implemented in a TMS320F28335 DSP+FPGA control board, and the sampling frequency is set to be 5 kHz.

VSG's main parameters are presented in Table I, D_p and K_q are chosen according to the grid codes like in [5], [12]. For this specific system, the worst-case is that the grid voltage drops to 0.6 p.u. and P_{ref}, Q_{ref} remain unchanged during the fault. Then, the transient responses of the worst-case are tested. In order to perform a comparative verification, different sets of J versus K_1 are examined. The corresponding experimental results are shown in Fig. 14 and Fig. 15. From top to bottom in each picture, the displayed waveforms are the grid voltage of phase a, i.e., V_{ga}, the line current of phase a, I_{ga}, the reactive and active power, Q and P, the deviation of VSG frequency $\Delta\omega$ and power angle δ, respectively.

In Case I, the system becomes unstable when V_g drops from 1 p.u. to 0.6 p.u. with J = 20 p.u.. Although the equilibrium point exists after the voltage sag, it is not reached due to the power angle's large overshoot. A low-frequency oscillation is triggered by the fault, which implies an instability caused by the

Fig.13. Control-hardware-in-loop platform used for the synchronization stability assessment of VSG.

TABLE I
Main Parameters of the VSG System Used in Experiments

Parameters	Description	Value	p.u.
P_{ref}	Rated active power	2.75 MW	1.0
Q_{ref}	Rated reactive power	0	0
V_0	Rated voltage	563 V	1.0
V_g	Normal grid voltage (line peak)	690 V	1.0
ω_0	Grid angular frequency	314 rad/s	1.0
L_g	Grid inductance	255 μH	0.46
D_p	Droop gain of *P-f*	8 P_{max}/ω_0	8
J	Virtual inertia	20 P_{max}/ω_0	20
K_q	*Q-V* droop gain	0.1V_0/Q_{max}	0.1
K_1	Damping coefficient	1 P_{max}/ω_0	1

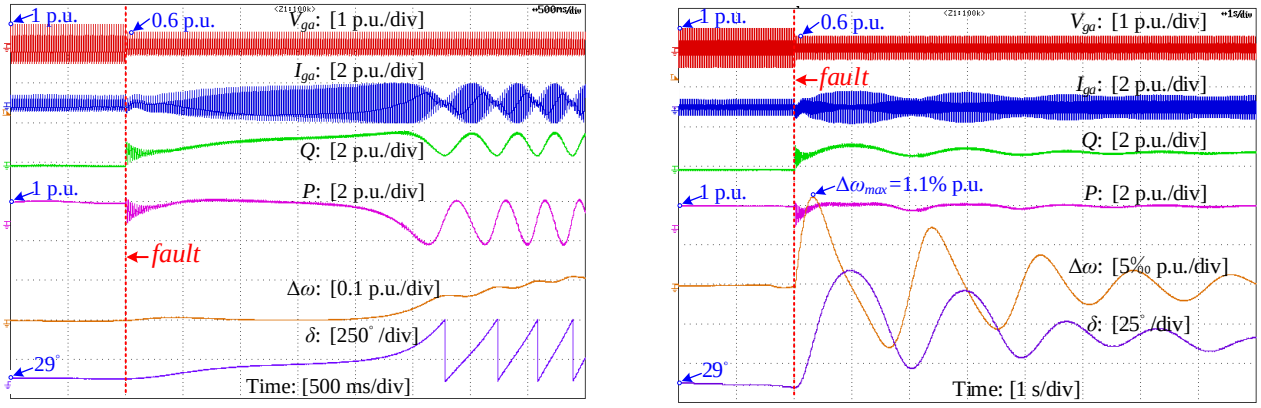

Fig. 14. Measured transient responses of the VSG without addtional damping path (K_1 = 0) when V_g dips from 1 p.u. to 0.6 p.u. (a) Case I: J = 20 p.u. and (b) Case II: J = 10 p.u..

This article has been accepted for publication in a future issue of this journal, but has not been fully edited. Content may change prior to final publication. Citation information: DOI 10.1109/TPEL.2020.3046462, IEEE Transactions on Power Electronics

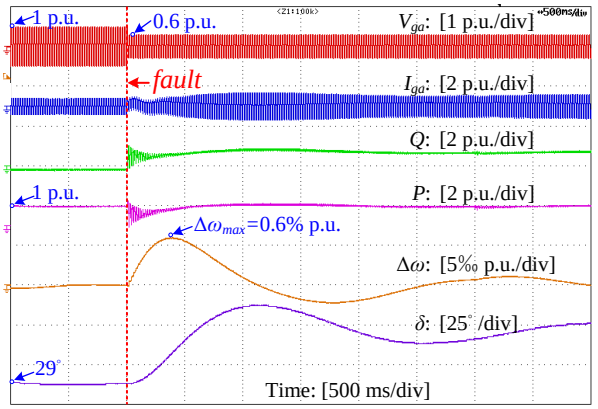

(a)

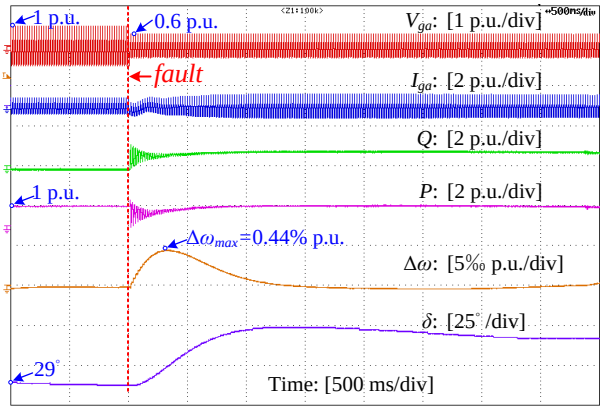

(b)

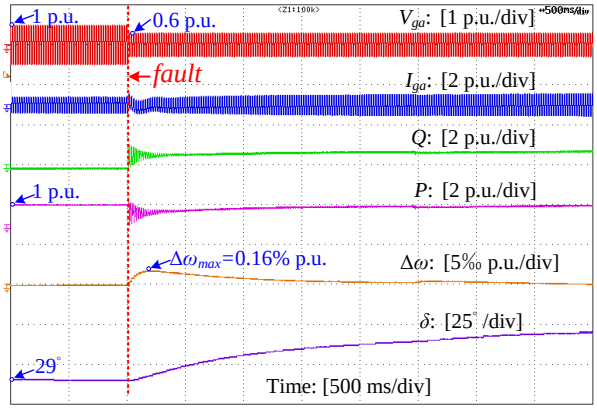

(c)

Fig. 15. Measured transient responses of the VSG with the addtional damping path in the active control loop and J = 20 p.u. when V_g dips from 1 p.u. to 0.6 p.u.. (a) Case III: K_1 = 20, (b) Case IV: K_1 = 60, (c) Case V: K_1 = 120.

lack of damping. On the contrary, a decrease of J is tested in Case II, i.e. J = 10 p.u., as shown in Fig. 14(b). Compared to Fig. 12, the system can be stable when SLG occurs, and even phase a is decreased to zero, indicating that the symmetrical grid faults are the most serious. Thus, the three-phase voltage sag is investigated in this paper. Under the same condition as in Fig 14(a), there is no additional damping path, and the instability in Fig. 14(a) is removed with a smaller J in Fig. 14(b), but it can be seen that $\Delta\omega_{max}$ and RoCoF are becoming larger. These results validate the theoretical analysis in Fig. 8, as shown with a red line there.

Next, introducing a transient-damping into the active power control loop is performed with different parameter settings in Fig. 15, respectively. From Fig. 15, it can be found that the additional transient damping path can stabilize the VSG when the grid voltage drops. The power angle overshoot declines with an increase of K_1. When K_1 = 120, almost no power angle overshoot can be found. The results agree with the theoretical analysis shown in Fig. 8 and Fig. 10.

Moreover, it can be clearly seen from Fig. 15 that with a larger K_1 not only reduces the power angle overshoot during the fault but also declines $\Delta\omega_{max}$. These experimental results are consistent with the theoretical analyzing results, confirming the transient-damping method's effectiveness in this paper, which has enhanced the synchronization stability of the VSG without degradation of the frequency stability.

VI. Conclusion

This paper has proposed a comprehensive method for analyzing VSG's dynamic performance during a large disturbance based on combining the linearized and nonlinear models. The method includes three steps: checking the existence of equilibrium points, then analyzing the small-signal stability, and finally analyze the transient behaviors during the fault. The relationship between the linearized and nonlinear models is first revealed, showing that the former is used for qualitative analysis to give precise physical insight. Simultaneously, the latter is adopted for quantitative analysis to assess stability after a grid fault. In order to avoid the conflict of the synchronization stability and the inertia response of the VSG, a transient damping method is added in the active power control loop. The damping ratio, power angle overshoot, and the maximum frequency variation during the fault are qualitatively interpreted based on a linearized model, indicating that the transient damping can increase the system's damping ratio, which can enhance the synchronization stability and frequency stability simultaneously. The parameter design guidelines are proposed to assess the synchronization stability with different inertia requirements based on a nonlinear model using the trajectories in the phase plane. It is found that a larger transient damping is expected with larger inertia. Finally, experimental results have verified the effectiveness of the combined analytical method, the transient damping method, and the parameters design method.

References

[1] J. Rocabert, A. Luna, F. Blaabjerg, and P. Rodriguez, "Control of power converters in ac microgrids," *IEEE Trans. Power Electron.*, vol. 27, no. 11, pp. 4734−4749, May 2012.

[2] Y. Deng, Y. Tao, G. Chen, G. Li, and X. He, "Enhanced power flow control for grid-connected droop-controlled inverters with improved stability," *IEEE Trans. Ind. Electron.*, vol. 64, no. 7, pp. 5919−5929, July 2017.

[3] J. M. Guerrero, L. G. de Vicuña, J. Matas, M. Castilla, and J. Miret, "A wireless controller to enhance dynamic performance of parallel inverters in distributed generation systems," *IEEE Trans. Power Electron.*, vol. 19, no. 5, pp. 1205−1213, Sep. 2004.

[4] L. Zhang, L. Harnefors, and H.-P. Nee, "Power-synchronization control of grid-connected voltage-source converters," *IEEE Trans. Power Syst.*,vol. 25, no. 2, pp. 809–920, May 2010.

[5] L. Harnefors, M. Hinkkanen, U. Riaz, F. M. M. Rahman and L. Zhang, "Robust Analytic Design of Power-synchronization control," *IEEE Trans. Ind. Electron*, vol. 66, no. 8, pp. 5810–5819, August 2019.

[6] J. Zhou, D. Hui, S. Fan, Y. Zhang, and A. M. Gole, "Impact of short circuit ratio and phase-locked-loop parameters on the small-signal behavior of a VSC-HVDC converter," *IEEE Trans. Power Del.*, vol. 29, no. 5, pp. 2287–2296, Oct. 2014.

[7] L. Harnefors, M. Bongiornos, and S. Lundberg, "Input-admittance calculation and shaping for controlled voltage-source converters," *IEEE Trans. Ind. Electron.*, vol. 54, no. 6, pp. 3323–3334, Dec. 2007.

[8] D. Pan, X. Wang, F. Liu and R. Shi, "Transient Stability of Voltage-Source Converters with Grid-Forming Control: A Design-Oriented Study," *IEEE J. Emerg. Sel. Topics Power Electron.*, vol. 8, no. 2, pp. 1019- 1033, June 2020.

[9] J. Fang, H. Li, Y. Tang and F. Blaabjerg, "Distributed power system virtual inertia implemented by grid-connected power converters," *IEEE Trans. Power Electron.*, vol. 33, no. 10, pp. 8488–8499, Oct. 2018.

[10] Q. C. Zhong and G. Weiss, "Synchronverters: inverters that mimic synchronous generators," *IEEE Trans. Ind. Electron.*, vol. 58, no. 4, pp. 1259−1267, Apr. 2011.

[11] Q. C. Zhong, P. L. Nguyen, Z. Ma, and W. Sheng, "Self-synchronized synchronverters: Inverters without a dedicated synchronization unit," *IEEE Trans. Power Electron.*, vol. 29, no. 2, pp. 617–630, Feb. 2014.

[12] H. Wu, X. Ruan, D. Yang, X. Chen, W. Zhao, Z. Lv and Q. C. Zhong, "Small-signal modeling and parameters design for virtual synchronous generators," *IEEE Trans. Ind. Electron.*, vol. 64, no. 7, pp. 4292–4303, Jul. 2016.

[13] J. Fang, Y. Tang, H. Li, and X. Li, "A battery/ultracapacitor hybrid energy storage system for implementing the power management of virtual synchronous generators," *IEEE Trans. Power Electron.*, vol. 33, no. 4, pp. 2820-2824, Apr. 2018.

[14] S. Dong and Y. C. Chen, "Adjusting synchronverter dynamic response speed via damping correction loop," *IEEE Trans. Energy Convers.*, vol. 32, no. 2, pp. 608–619, Jun. 2017.

[15] H. Wu and X. Wang, "A mode-adaptive power-angle control method for transient stability enhancement of virtual synchronous generators," *IEEE J. Emerg. Sel. Topics Power Electron.*, vol. 8, no. 2, pp. 1034- 1049, Jun. 2020.

[16] Z. Shuai, C. Shen, X. Liu, Z. Li and Z. J. Shen, "Transient angle stability of virtual synchronous generators using Lyapunov's direct method," *IEEE Trans. Smart Grid.*, vol. 10, no. 4, pp. 4648- 4661, Aug. 2018.

[17] H. Cheng, Z. Shuai, C. Shen, X. Liu, Z. Li and Z. J. Shen, "Transient angle stability of paralleled synchronous and virtual synchronous generators in islanded microgrids," *IEEE Transactions on Power Electronics*, vol. 35, no. 8, pp. 8751-8765, Aug. 2020.

[18] H. Wu and X. Wang, "Design-oriented transient stability analysis of grid connected converters with power synchronization control" *IEEE Trans. Ind. Electron.*, vol. 66, no. 8, pp. 6473–6482, Aug. 2019.

[19] L. Zhang, L. Harnefors, and H.-P. Nee, "Interconnection of two very weak AC systems by VSC-HVDC links using power-synchronization control," *IEEE Trans. Power Syst.*, vol. 26, no. 1, pp. 344−355, Feb. 2011.

[20] P. Pan, W. Chen, L. Shu, H. Mu, K. Zhang, M. Zhu, F. Deng, "An impedance-based stability assessment methodology for DC distribution power system with multivoltage levels," *IEEE Trans. Power Electron.*, vol. 35, no. 4, pp. 4033-4047, April 2020.

[21] X. Xiong and X. Ruan, "Non-smooth bifurcation analysis of multi-structure multi-operating-mode power electronics systems for applications with renewable energy sources," *IEEE Trans. Circuits Syst. II，Exp. Briefs*, 2019, vol. 66, no. 3, pp. 487-491.

[22] L. Harnefors, X. Wang, A. Yepes, and F. Blaabjerg, "Passivity-based stability assessment of grid-connected VSCs - an overview," *IEEE Jour. Emer. Select. Top. Power Electron.*, vol. 4, no. 1, pp. 116-125, Mar. 2016.

[23] H. Yuan, X. Yuan, and J. Hu, "Modeling of grid-connected VSCs for power system small-signal stability analysis in DC-link voltage control timescale," *IEEE Trans. Power Syst.*, vol. 32, no. 5, pp. 3981−3991, Sep. 2017.

[24] D. Dong, B. Wen, D. Boroyevich, P. Mattavelli, and Y. Xue, "Analysis of phase-locked loop low-frequency stability in three-phase grid-connected power converters considering impedance interactions," *IEEE Trans. Ind. Electron.*, vol. 62, no. 1, pp. 310–321, Jan. 2015.

[25] O. Göksu, R. Teodorescu, C. L. Bak, F. Iov, and P. C. Kjær, "Instability of wind turbine converters during current injection to low voltage grid faults and PLL frequency based stability solution," *IEEE Trans. Power Syst.*, vol. 29, no.4, pp. 1683–1691, Jul. 2014.

[26] M. G. Taul, X. Wang, P. Davari and F. Blaabjerg, "Systematic approach for transient stability evaluation of grid-tied converters during power system faults," in *Proc. IEEE Energy Conversion Congress and Exposition*, Baltimore, MD, USA, pp. 5191–5198, Sep. 2018.

[27] J. Zhao, M. Huang, H. Yan, C. K. Tse and X. Zha, "Nonlinear and transient stability analysis of phase locked loops in grid-connected converters," *IEEE Trans. Power Electron.*, vol. 36, no.1, pp. 1018-1029, Jan. 2021.

[28] Y. W. Li and C.-N. Kao, "An accurate power control strategy for power electronics-interfaced distributed generation units operating in a low voltage multi bus microgrid," *IEEE Trans. Power Electron.*, vol. 24, no.12, pp. 2977-2988, Dec. 2009.

[29] X. Yan and S. Y. A. Mohamed, "Comparison of virtual synchronous generators dynamic responses," *2018 IEEE 12th International Conference on Compatibility, Power Electronics and Power Engineering* , Doha, 2018, pp. 1-6.

[30] M. Ebrahimi, S. A. Khajehoddin, and M. K.-Ghartemani, "An improved damping method for virtual synchronous machines," *IEEE Trans. Sustain. Energy*, vol. 10, no. 3, pp. 1491−1500, Jul. 2019.

[31] O. Mo, S. D'Arco, and J. A. Suul, "Evaluation of virtual synchronous machines with dynamic or quasi-stationary machine models," *IEEE Trans. Ind. Electron.*, vol. 64, no. 7, pp. 5952−5962, Jul. 2017.

[32] J. A. Suul, S. D'Arco, and G. Guidi, "Virtual synchronous machine based control of a single-phase bi-directional battery charger for providing vehicle-to-grid services," *IEEE Trans. Ind. Appl.*, vol. 52, no. 4, pp. 3234–3244, Jul./Aug. 2016.

[33] Z. Shuai, W. Huang, Z. John Shen, A. Luo, and Z. Tian, "Active power oscillation and suppression techniques between two parallel synchronverters during load fluctuations," *IEEE Trans. Power Electron.*, vol. 35, no.4, pp. 4127-4142, Apr. 2020.

[34] M. G. Taul, S. Golestan, X. Wang, P. Davari and F. Blaabjerg, "Modeling of converter synchronization stability under grid faults: the general case," *IEEE J. Emerg. Sel. Topics Power Electron.*, 2020, early access.

Xiaoling Xiong (M'19) received the B.S., M.S. and Ph.D degrees in electrical engineering from Nanjing University of Aeronautics and Astronautics, Nanjing, China, in 2007, 2010 and 2015 respectively. She had worked as a Research Assistant in Department of Electronic and Information Engineering at Hong Kong Polytechnic University from February, 2011 to July, 2012.

Since 2015, she has been with North China Electric Power University, Beijing, where she was a lecturer. Simultaneously, she has been with Aalborg University, Aalborg, Denmark from December, 2018 to November, 2020, where she was a visiting Post-Doctoral with the Department of Energy Technology. Her current research interests include HVDC system, modeling, analysis and design power electronic systems and study the nonlinear behaviors in power electronic circuits.

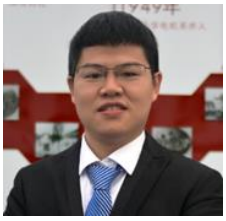

Chao Wu (M'19) was born in Hubei Province, China. He received the B.Eng. degree from HeFei University of Technology, Hefei, China and the Ph.D. degree from Zhejiang University, Hangzhou, China, in 2014 and 2019, both in electrical engineering. He is currently a Postdoctoral Researcher in the Department of Energy Technology, Aalborg University, Aalborg, Denmark.

His current research interests include cooperative control of multi-converter systems, particularly the control and operation of doubly fed induction generators for DC connection and the transient stability of power converters.

Bin Hu was born in Wenzhou, China. He received the B.Eng. degree in electrical engineering from Shenyang University of Technology, Shenyang, China, in 2018. He is currently working towards the Ph.D. degree of electrical engineering in Zhejiang University.

His research interests include the phase-locked synchronization methods for wind power generation system under weak grid, their impedance characteristic analysis and reshaping control strategy.

Donghua Pan (S'12-M'15) received the B.S. and Ph.D. degrees in electrical engineering from Huazhong University of Science and Technology, Wuhan, China, in 2010 and 2015, respectively.

From July 2015 to August 2017, he was a Research Engineer with Suzhou Inovance Technology Co., Ltd., Suzhou, China. From September 2017 to October 2019, he was a Postdoctoral Fellow with the Department of Energy Technology, Aalborg University, Aalborg, Denmark. His research interests include magnetic integration techniques, modeling and control of grid-connected converters, and wide bandgap power conversion systems.

Dr. Pan was the recipient of the Outstanding Reviewer Award of IEEE Transactions on Power Electronics in 2017 and the Best Paper Award at IEEE SPEC 2018.

Frede Blaabjerg (S'86–M'88–SM'97–F'03) was with ABB-Scandia, Randers, Denmark, from 1987 to 1988. From 1988 to 1992, he got the PhD degree in Electrical Engineering at Aalborg University in 1995. He became an Assistant Professor in 1992, an Associate Professor in 1996, and a Full Professor of power electronics and drives in 1998. From 2017 he became a Villum Investigator. He is honoris causa at University Politehnica Timisoara (UPT), Romania and Tallinn Technical University (TTU) in Estonia.

His current research interests include power electronics and its applications such as in wind turbines, PV systems, reliability, harmonics and adjustable speed drives. He has published more than 600 journal papers in the fields of power electronics and its applications. He is the co-author of four monographs and editor of ten books in power electronics and its applications.

He has received 32 IEEE Prize Paper Awards, the IEEE PELS Distinguished Service Award in 2009, the EPE-PEMC Council Award in 2010, the IEEE William E. Newell Power Electronics Award 2014, the Villum Kann Rasmussen Research Award 2014, the Global Energy Prize in 2019 and the 2020 IEEE Edison Medal. He was the Editor-in-Chief of the IEEE TRANSACTIONS ON POWER ELECTRONICS from 2006 to 2012. He has been Distinguished Lecturer for the IEEE Power Electronics Society from 2005 to 2007 and for the IEEE Industry Applications Society from 2010 to 2011 as well as 2017 to 2018. In 2019-2020 he serves a President of IEEE Power Electronics Society. He is Vice-President of the Danish Academy of Technical Sciences too.

He is nominated in 2014-2019 by Thomson Reuters to be between the most 250 cited researchers in Engineering in the world.